Radka Kodešová*
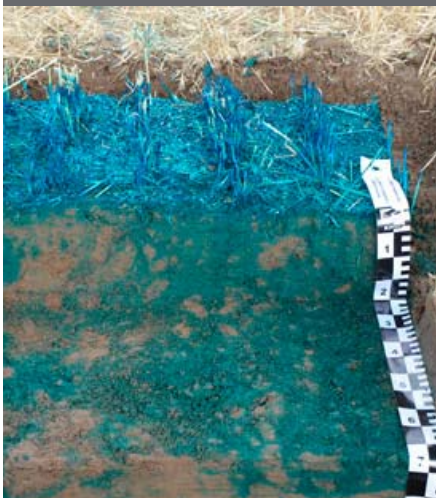**Jiří Šimůnek**
Antonín Nikodem
Veronika Jirků

Hydraulic and mass exchange term parameters for the HYDRUS 2D/3D dual-permeability model were estimated using data from micromorphological images and dye tracer experiments, and numerical inversion of transient infiltration data measured with tension disk infiltrometer and Guelph permeameter methods in the surface horizon of Haplic Luvisol.

R. Kodešová, A. Nikodem, V. Jirků, Czech Univ. of Life Sciences Prague, Faculty of Agrobiology, Food and Natural Resources, Dep. of Soil Science and Soil Protection, Kamýcká 129, 16521 Prague 6, Czech Republic; and J. Šimůnek, Dep. of Environmental Sciences, 900 University Av., Univ. of California, Riverside, CA 92521. *Corresponding author (kodesova@af.czu.cz).

Estimation of the Dual-Permeability Model Parameters using Tension Disk Infiltrometer and Guelph Permeameter

A determination of the parameters describing the soil hydraulic properties of matrix and macropore domains and mass exchange between these domains is crucial when preferential water flow in structured soils is simulated using the dual-permeability model. This study focused on estimating the parameters of the radially symmetric dual-permeability model from cumulative infiltration measured in the surface horizon of a Haplic Luvisol. While parameters obtained from the numerical inversion of the tension disk infiltration, using the single-porosity flow model in HYDRUS 2D/3D, were used to describe the matrix domain, the parameters characterizing the macropore domain and mass exchange between domains were estimated using the Guelph permeameter infiltration and the dual-permeability flow model in HYDRUS 2D/3D. The mass transfer coefficient between the two pore domains affected the simulated water regime considerably, and subsequently, the calibrated value of the saturated hydraulic conductivity in the macropore domain, K_{sf}. A less significant impact of the aggregate shape factor was observed due to a low range of possible values compared with the other two parameters, which either varied within orders of magnitude (the effective saturated hydraulic conductivity of the interface between the two pore domains, K_{sa}) or were squared (the characteristic length of an aggregate, a). The K_{sf} values increased when mass exchange decreased (when a increased and K_{sa} decreased). Since both parameters are mutually correlated and therefore have a similar impact on simulated data, we suggest that a be determined independently, and K_{sa} and K_{sf} should be simultaneously optimized when the parameters of the dual-permeability model are evaluated using the presented experimental procedure.

Abbreviations: MSO, multistep outflow; PI, ponding infiltration.

Soil and groundwater contamination by various chemicals used in agriculture and industry present a serious environmental problem that has been widely studied. Review studies by Šimůnek et al. (2003), Gerke (2006), Jarvis (2007), Clothier et al. (2008), Šimůnek and van Genuchten (2008), and Köhne et al. (2009a,b) have summarized and documented that water flow and contaminant transport in soils is frequently influenced by either water and solute temporal immobilization or preferential flow. Many numerical models have been developed to describe such nonequilibrium water flow and solute transport in soils. Commonly used physically based models simulating water flow and solute transport in soils use either single continuum or bi- and multicontinuum approaches. Bi- and multimodal concepts assume that the soil porous system is divided into two (or more) domains, while each domain is characterized by its own set of transport properties and equations for describing local flow and transport processes. Only two-domain models have been widely tested, however.

The dual-porosity (mobile–immobile) approach (Philip, 1968; Šimůnek et al., 2003) describes water flow and solute transport in systems consisting of domains with both mobile and immobile water. The dual-porosity formulation is based on a set of equations describing water flow and solute transport in the mobile domain (Richards and advection–dispersion equations), with mass balance equations describing soil water and solute contents in the immobile domain. The dual-permeability approach assumes that water flow and solute transport occur in both domains. The dual-permeability formulation is based on a set of equations that describe water flow and solute transport separately in each domain (the matrix and macropore domains). While the Richards equation is typically used to describe water flow in the matrix domain, various equations are used to describe water flow in the macropore domain (Šimůnek et al., 2003; Gerke, 2006). The gravity-driven kinematic

wave approach was applied by Germann (1985), Germann and Beven (1985), and Jarvis (1994). The Richards equation was used by Othmer et al. (1991) and Gerke and van Genuchten (1993, 1996). There are also other approaches describing preferential flow in discrete macropores, which are based on Poiseuille's equation (Ahuja and Hebson, 1992), boundary layer theory for viscous flow (Germann, 1990), and the Chezy–Manning equation for turbulent flow in macropores (Chen and Wagenet, 1992a). The transport in the macropore domain can be described using either the advection–dispersion equation (Gerke and van Genuchten, 1993) or a piston-type transport (Jarvis, 1994).

There are also many approaches for describing water and solute transfer between the mobile and immobile domains and between the macropore and matrix domains (Šimůnek et al., 2003; Gerke, 2006). Pressure-head-based (Gerke and van Genuchten, 1993; Zimmerman et al., 1996) or saturation-based (Philip, 1968; Šimůnek et al., 2003; Jarvis, 1994) mass transfer terms may be used to describe water transfer. The Green–Ampt infiltration equation (Ahuja and Hebson, 1992), the Philip infiltration equation (Chen and Wagenet, 1992a), or the Richards equation (Chen and Wagenet, 1992b) are applied to simulate water infiltration from the discreet macropores into the matrix. Depending on the mass transfer model used to describe water flow, diffusion or advection mass transfer terms are used to describe solute transfer.

The HYDRUS-1D and HYDRUS 2D/3D codes (Šimůnek et al., 2008), which were used in this study, include single-porosity, dual-porosity, and dual-permeability models all based on the numerical solution of the Richards and advection–dispersion equations for different flow domains. Pressure-head-based or saturation-based mass transfer terms are used to characterize water transfer between the mobile and immobile domains. Pressure-based terms are applied for simulating water transfer between the macropore and matrix domains of the dual-permeability model.

To apply two- (or multi-) domain models, the domain fractions and the properties characterizing water flow and solute transport within and between the domains must be specified. Numerical inversion of the observed water flow and tracer transport data is usually used to obtain the desired information (see review articles referenced above); however, many parameters must be measured independently or determined from the literature to obtain reliable results. A summary of the various approaches for independent parameter determination was given by Köhne et al. (2009a). The hydraulic parameters of multimodal soil porous systems are usually determined based on the transient flow and transport data obtained under various laboratory conditions (Pot et al., 2005; Köhne et al., 2006a,b; Kodešová et al., 2006a, 2008, 2009).

Tension disk infiltrometers and Guelph permeameters are frequently used to measure the unsaturated, $K(h)$, and saturated, K_s, hydraulic conductivities of the three-dimensional soil–pore system in the field.

The analytical expressions presented by Wooding (1968) and Zhang et al. (1998) are usually used to calculate K values from the tension disk infiltrometer and the Guelph permeameter, respectively. An inversion of models based on the numerical solution of the Richards equation and the van Genuchten–Mualem expressions describing soil hydraulic properties has also been applied to evaluate the other soil hydraulic parameters from the tension disk infiltrometer transient flow data (Šimůnek and van Genuchten, 1996, 1997; Schwartz and Evett, 2002; Ramos et al., 2006).

On the other hand, data obtained using the Guelph permeameter have not yet been numerically analyzed to estimate soil hydraulic parameters. Numerical simulations have been used only to define the shape factor, which was utilized in the analytical evaluation of the saturated hydraulic conductivity (Hayashi and Quinton, 2004); however, parameter estimation was applied to a new tool called a Restricted Interval Guelph permeameter (Freifeld and Oldenburg, 2000). Numerical inversion was also utilized to evaluate the soil hydraulic parameters from a cone permeameter experiment (Kodešová et al., 1998, 1999; Šimůnek et al., 1999), which had a geometry of the flow domain similar to the Guelph permeameter experiment. None of these studies assumed nonequilibrium water flow.

The main objective of this study was to take advantage of different boundary flow conditions applied during tension disk infiltrometer (performed under unsaturated conditions) and Guelph permeameter (performed under ponding infiltration conditions) experiments to assess preferential flow in macropores, i.e., pores with diameters larger than the diameter corresponding to the applied pressure head of the tension disk infiltrometer. The single-porosity and dual-porosity models in HYDRUS 2/3D were applied to estimate the parameters of the soil hydraulic functions of both models using the tension disk infiltrometer and the Guelph permeameter transient flow data. The goals of this study were: (i) assessment of the impact of various retention curve parameters (obtained independently using two different laboratory methods) on optimized K_s using the single-porosity model for both field experiments; (ii) evaluation of the possible influence of macropores on water flow and, consequently, on the estimated values of the K_s by comparing the optimized values obtained using the single-porosity model and different field experiments (disk or permeameter); (iii) Estimation of the K_{sf} value for the macropore domain of the dual-permeability model using the Guelph permeameter transient flow data. In the case of this third goal, the soil hydraulic parameters obtained using the tension disk infiltrometer data were assumed to characterize the matrix domain. The parameters characterizing dual-domain geometry, water retention in the macropore domain, and the hydraulic conductivity of the interface between the macropore and matrix domains were also unknown and had to be estimated. Therefore, additional goals of this study were: (iv) evaluation of the impact of various parameters describing aggregate structure on the estimated K_{sf} values; (v) evaluation

of the influence of various soil water retention parameters in the macropore domain on the estimated K_{sf} values; and (vi) evaluation of the impact of various effective saturated hydraulic conductivities of the interface between the macropore and matrix domains on the estimated K_{sf} values.

Materials and Methods
Field Experiments

The study was performed at the experimental station of the Crop Research Institute in Hněvčeves, the Czech Republic. The soil studied was Haplic Luvisol (loess parent material). Four soil diagnostic horizons were identified in the soil profile: Ap, 0 to 35 cm; Bt1, 35 to 57 cm; Bt2, 57 to 93 cm; and Ck, 93 to 129 cm. Conventional tillage was used at this location. Crops were planted within small areas that allowed the soil properties to be studied every year under similar conditions. Despite a 5-yr rotation system, the properties were studied using the same crop (winter barley [*Hordeum vulgare* L.] or wheat [*Tritcum aestivum* L.]) and with a reasonable distance between the sampling and experimental plots.

Before the study began, the hydraulic properties of the diagnostic horizons were studied in the laboratory using multistep outflow experiments performed on undisturbed 100-cm^3 soil samples (soil core height of 5.1 cm and cross-sectional area of 19.60 cm^2) (Kodešová et al., 2008). Initially, fully saturated soil samples placed in the Tempe cells were slowly drained using nine pressure head steps (a minimum pressure head of −1000 cm) during a 3-wk period. Ponding infiltration tests on undisturbed 1125-cm^3 soil columns (soil core height of 13 cm and cross-sectional area of 86.54 cm^2) were then performed to study the hydraulic properties of different diagnostic horizons (Kodešová et al., 2009). The ponding depth was 1.5 cm, and the experiments lasted 150 min. In both studies, micromorphological images were used to evaluate the macroporosity, which was defined as pores with diameters >40 µm.

The single- and dual-porosity models in HYDRUS-1D (Šimůnek et al., 2008) were successfully applied to simulate water flow in the Ap1, Ap2, and Bt1 horizons for the multistep outflow experiments (experiments performed mostly under unsaturated conditions) and to optimize the soil hydraulic parameters in all mobile domains. The single-porosity and dual-permeability models in HYDRUS-1D were used to simulate water flow in the Ap, Bt1, and Bt2 horizons under ponding infiltration conditions (experiments involving both unsaturated and saturated conditions) and to estimate the soil hydraulic parameters and solute transport parameters in all domains. While the dual-permeability model, in combination with information obtained from the micromorphological images, successfully described water flow and solute transport in the subsurface horizons, it was less successful for describing flow in the Ap horizon. An analysis of the soil pores showed bimodality in the detected macropore system, with a high fraction of gravitational pores. The influence of the gravitational pores on the observed water flow and solute transport could not be simulated successfully using the assumption of one macropore domain representing both large capillary and gravitational pores. To remedy this, new experiments were performed directly in the field to assess this phenomenon.

Field experiments were performed immediately after the harvest of winter barley in 2008 (at approximately the time of the previous years' sampling), at a close distance from the previous years' sampling plots. Measurements were performed randomly within an area of 10 m^2, avoiding the locations impacted by either the wheels of heavy machinery or by the experimental work performed in the area. A tension disk infiltrometer (with a disk radius of 10 cm) was used to measure the cumulative water infiltration under unsaturated conditions created using a pressure head of −2 cm (Watson and Luxmoore, 1986). Measurements were performed at a depth of 5 cm. A Guelph permeameter was used to measure the cumulative water flux under surface ponding conditions. The depth of the drilled well was 10 cm, the well radius was 3 cm, and the well ponding depth was 5 cm. The depths of the experiments were selected based on the following observations: (i) it was observed in the field that after excluding the top 1 cm of the soil crust, the humic Ap horizon was relatively homogeneous to a depth of 25 cm; (ii) water flow under the tension disk infiltrometer was mostly downward but also horizontal and therefore the wetted domain was expected to be between depths of 5 and approximately 15 cm; and (iii) using the Guelph permeameter, water flow is downward, horizontal, and also upward and therefore the wetted domain was expected to be between depths of 1 cm (i.e., above a depth of 5 cm, which was the position of a water table in the well) and 20 cm. The maximum wetted horizontal cross-section was expected to be similar to the area of the disk infiltrometer.

The soil surface was carefully leveled using a sharp knife before the tension disk infiltrometer tests. Then, a 1-mm layer from the same soil, sieved through a 2-mm sieve, was formed to ensure close contact between the soil and the disk. The standard procedure recommended in the Guelph permeameter manual (Soilmoisture Equipment Corp., 2008) was used to prepare the infiltration well. A soil auger was used to drill the well to the desired depth. A sizing auger was used for the final well shaping, and the well brush was applied to remove the smear layer on the well sides. The tension disk infiltrometer tests lasted at least 60 min and the Guelph permeameter tests at least 30 min. Data were collected manually. Cumulative infiltration was measured using a Mariotte tube (shaded from sunlight if necessary), and times were measured with a stopwatch. The results of three replicates with each permeameter are presented here.

A dye infiltration experiment was performed in 2009, using a procedure similar to that described by Sander and Gerke (2007). One hundred liters of solution with the food color Brilliant Blue FCF (5 kg m^{-3}) was infiltrated into a 1- by 1-m plot (applying an initial ponding depth of 10 cm) immediately after wheat harvest. On the

next day, one half of the plot was sliced horizontally and the other half vertically to study the dye distribution in the soil profile to a depth of 100 cm. An example of a staining pattern within the vertical and horizontal (to a depth of 20 cm) sections is shown in Fig. 1 and was used to estimate the dual-domain geometry. Figure 1 shows that a less permeable crust layer 1 cm thick reduced water and dye infiltration at the top of the surface Ap1 horizon (0–25 cm). Below the crust layer, the dye tracer was transported mostly regularly, and only some isolated uncolored domains were visible in this horizon. The dye transport in the Ap2 horizon (25–35 cm, the plow pan) slowed down due to the very compact matrix structure. The dye transport through the plow pan was caused mainly by gravitational biopores.

Water Flow Models

The single-porosity and dual-permeability models implemented in HYDRUS 2D/3D (Šimůnek et al., 2008) were used to simulate the observed cumulative water fluxes and to estimate the soil hydraulic parameters via numerical inversion. The Richards equation, which describes isothermal Darcian flow in a variably saturated rigid porous medium, is used in both models. The flow domain was assumed to be isotropic, as previous micromorphological studies (Kodešová et al., 2008, 2009) showed that the soil material consisted of regular angular blocky soil aggregates without layering or other features that could cause anisotropic conditions. The Richards equation for the radially symmetric, single-porosity system may be applied to simulate both transient experiments:

$$\frac{\partial \theta}{\partial t} = \frac{1}{r}\frac{\partial}{\partial r}\left[rK(h)\frac{\partial h}{\partial r}\right] + \frac{\partial}{\partial z}\left[K(h)\frac{\partial h}{\partial z} + K(h)\right] \qquad [1]$$

where θ is the volumetric soil water content [L^3 L^{-3}], h is the pressure head [L], K is the hydraulic conductivity [L T^{-1}], t is time [T],
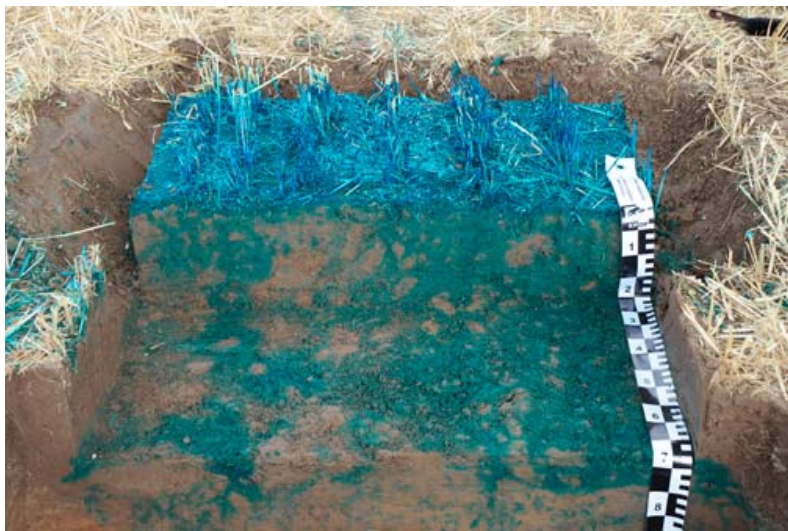
r is the radial coordinate [L], and z is the vertical axis [L]. Equation [1] is solved for the entire flow domain using one set of soil water retention and hydraulic conductivity functions.

In the dual-permeability model, the Richards equation is applied separately to each of the two pore regions, i.e., the macropore (fractures, a domain of larger pores) and matrix domains (Gerke and van Genuchten, 1993). The Richards equation for the radially symmetric, dual-permeability system may be written as

$$\frac{\partial \theta_f}{\partial t} = \frac{1}{r}\frac{\partial}{\partial r}\left[rK_f(h_f)\frac{\partial h_f}{\partial r}\right]$$
$$+ \frac{\partial}{\partial z}\left[K_f(h_f)\frac{\partial h_f}{\partial z} + K_f(h_f)\right] - \frac{\Gamma_w}{f_w}$$
$$\frac{\partial \theta_m}{\partial t} = \frac{1}{r}\frac{\partial}{\partial r}\left[rK_m(h_m)\frac{\partial h_m}{\partial r}\right] \qquad [2]$$
$$+ \frac{\partial}{\partial z}\left[K_m(h_m)\frac{\partial h_m}{\partial z} + K_m(h_m)\right] + \frac{\Gamma_w}{1 - f_w}$$

where the subscripts f and m refer to the macropore and matrix domains, respectively, Γ_w is the mass transfer term for water exchange between the macropore and matrix domains [T^{-1}], and f_w is the macropore domain fraction (dimensionless), i.e., the ratio of the volumes of the macropore and total flow domains. The matrix domain fraction is specified as $1 - f_w$. Equations [2] are solved using two sets of soil water retention and hydraulic conductivity functions, which are defined for each domain. The total soil water content and the hydraulic conductivity are defined as the sum of the soil water contents or hydraulic conductivities of each domain multiplied by corresponding domain fractions.

The mass exchange between the matrix and macropore regions, Γ_w, is calculated as

$$\Gamma_w = \frac{\beta}{a^2}\gamma_w K_a(h_a)(h_f - h_m)$$
$$\text{and} \qquad [3]$$
$$K_a(h_a) = K_{sa}K_{rm}(h_a)$$

where K_a is the effective hydraulic conductivity of the interface between the two pore domains [L T^{-1}], K_{sa} is the saturated hydraulic conductivity of the interface, $K_{rm}(h_a)$ is the matrix relative unsaturated hydraulic conductivity function calculated using the van Genuchten model (see below), and h_a is the pressure head at the interface [taken as $(h_f + h_m)/2$]. The parameters describing the aggregate shapes (Gerke and van Genuchten, 1996) are the dimensionless shape factor β (15 for spherical aggregates, 3 for cubic aggregates), the characteristic length of an aggregate, a [L] (a sphere radius or half size of the cube edge), and the dimensionless scaling factor γ_w (= 0.4).

Fig. 1. Distribution of Brilliant Blue FCF dye within the Ap1 and Ap2 horizons after infiltration in a 1- by 1-m plot.

The analytical expressions proposed by van Genuchten (1980) for the soil water retention curve, $\theta(h)$, and the hydraulic conductivity function, $K(\theta)$, are used in both models:

$$\theta_e = \frac{\theta(h) - \theta_r}{\theta_s - \theta_r} = \frac{1}{\left(1 + |\alpha h|^n\right)^m} \quad h < 0$$
$$\theta_e = 1 \qquad\qquad\qquad\qquad h \geq 0 \tag{4}$$

$$K(\theta) = K_s \theta_e^l \left[1 - \left(1 - \theta_e^{1/m}\right)^m\right]^2 \quad h < 0$$
$$K(\theta) = K_s \qquad\qquad\qquad\qquad h \geq 0 \tag{5}$$

where θ_e is the effective soil water content (dimensionless), K_s is the saturated hydraulic conductivity [L T^{-1}], θ_r and θ_s are the residual and saturated soil water contents [L^3 L^{-3}], respectively, l is the pore-connectivity parameter (dimensionless), α is the reciprocal of the air-entry pressure head [L^{-1}], n (dimensionless) is related to the slope of the retention curve at the inflection point, and $m = 1 - 1/n$.

Soil Hydraulic Parameter Estimation

First, the single-porosity model was applied to estimate the soil hydraulic parameters of the Ap1 horizon from the cumulative water infiltration measured using both the tension disk infiltrometer and the Guelph permeameter. The finite element mesh for an axisymmetrical quasi-three-dimensional flow domain is shown in Fig. 2 for the Guelph permeameter. The flow domain either contained an axisymmetrical well of a radius of 3 cm and a depth of 10 cm for the Guelph permeameter or was flat at the top for the tension disk infiltrometer (not shown). The right side and bottom boundaries of both flow domains were set far enough away so as

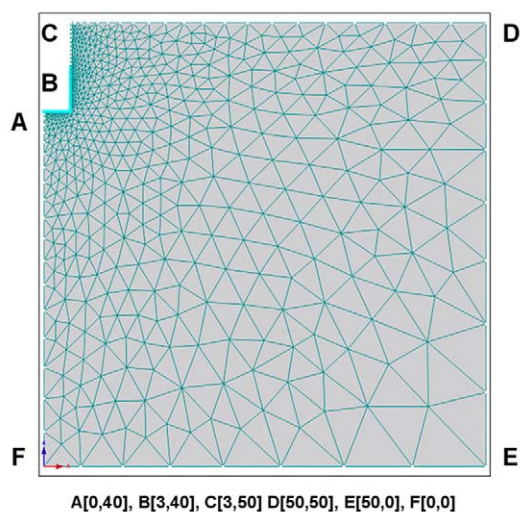A[0,40], B[3,40], C[3,50] D[50,50], E[50,0], F[0,0]

Fig. 2. A finite element mesh generated for the Guelph permeameter experiments. Coordinates are in centimeters. Blue nodes at the boundary represent a constant-head boundary condition. Coordinates of the A, B, C, D, E, and F points in the radially symmetric system are in centimeters.

not to influence the simulated transient flow data. An entire simulated domain was assumed to consist of only a single material. The initial conditions were specified using pressure heads that were calculated for the average measured initial soil water content (0.33 cm^3 cm^{-3}) using the applied soil water retention curve (which is specified below). A constant pressure head of -2 cm was set at the boundary where the tension disk infiltrometer came into contact with the soil. A constant hydrostatic pressure head (5 cm at the bottom) was set at the boundary where ponding infiltration was applied for the Guelph permeameter. A free-drainage boundary condition was specified at the bottom of the transport domain. Because it was assumed that boundary conditions at the remaining domain boundaries do not affect the simulated flow, a zero-flux boundary condition was set at these boundaries (see, for instance, Šimůnek and van Genuchten, 1996, 1997; Šimůnek et al., 1999; Kodešová et al., 1998, 1999).

Because it has been shown that cumulative infiltration for the one-step disk infiltrometer experiment without additional transient flow data does not provide enough information for the numerical optimization of all soil hydraulic parameters (Šimůnek and van Genuchten, 1996), the following simplifications were used. The parameters of the soil water retention curve (θ_r, θ_s, α, and n) were set to values obtained in previous studies (Table 1) performed on the same soil. In these studies, multistep outflow (MSO) experiments (Kodešová et al., 2008) and ponding infiltration (PI) tests (Kodešová et al., 2009) were analyzed using the HYDRUS-1D single-porosity model. It should be mentioned that while the parameters θ_r, α, n, and K_s were optimized via numerical inversion of both the MSO and PI transient flow data, the saturated water contents θ_s were set to measured values. The θ_s value for the MSO data analysis was obtained from a saturation pan. The θ_s value for the PI data analysis was equal to the sample porosity. A lower θ_s value for the MSO test compared with that obtained for the PI test resulted because samples are usually taken in such a way as to avoid large (gravitational) pores or cracks, and the probability that large pores or cracks are present in the soil core increases with its size. Thus, a smaller fraction of macropores could be included in smaller samples, resulting in a lower value of the sample porosity compared with that in larger soil samples (100- vs. 1125-cm^3 soil samples). In addition, the θ_s value obtained from the saturation pan might have been slightly lower than the actual sample porosity. The values of the α and n parameters ($\alpha_{MSO} < \alpha_{PI}$ and $n_{MSO} < n_{PI}$) indicate

Table 1. Soil hydraulic parameters (van Genuchten, 1980) obtained in previous studies.

Experiment	θ_r	θ_s	α	n	K_s
	—— cm^3 cm^{-3} ——		cm^{-1}		cm min^{-1}
Ponding infiltration†	0	0.428	0.0124	2.001	0.0377
Multistep outflow‡	0.217	0.363	0.0072	1.758	3.12×10^{-4}

† Kodešová et al. (2009).
‡ Kodešová et al. (2008).

that the shape of the soil water retention curve obtained from the MSO test is more gradual than that obtained from the PI test. Note that α from the wetting experiment (PI) is larger than from the drying experiment (MSO), while the n values are relatively similar, as would be expected considering the hysteresis model of Kool and Parker (1987). Parameters resulting from different experiments were chosen to assess the impact of various phenomena, such as different experimental history (drying vs. wetting experiments) and flow conditions (mostly unsaturated vs. mostly saturated), on optimized K_s values. The value of l was set equal to 0.5 (Mualem, 1976). Saturated hydraulic conductivities, K_s, were optimized via numerical inversion using the single-porosity model in HYDRUS 2D/3D. The same procedure was applied to analyze the cumulative infiltration measured using the Guelph permeameter.

Next, the dual-permeability model in HYDRUS 2D/3D was used to analyze the cumulative infiltration measured using the Guelph permeameter. The same finite element mesh as was used for the single-porosity model was utilized, and the same boundary conditions were applied for both domains. The initial conditions were set similar to those set for the single-porosity model. To have initially no mass transfer between the two domains, the same pressure head was specified in both domains. The initial pressure heads were calculated using the applied soil water retention curves (which are specified below for each scenario; Tables 1 and 2), assuming that the sum of the initial soil water contents in both domains multiplied by their domain fractions equals the average measured initial soil water content (0.33 cm^3 cm^{-3}). The fraction of the macropore domain (f_w = 0.0277) was determined, based on the micromorphological study of Kodešová et al. (2009), as the ratio of the image porosity for pores >1000 µm (0.0119) and the sample porosity (0.428).

Parameters characterizing the aggregate geometry were set based on the study of Kodešová et al. (2006b), the micromorphological studies of Kodešová et al. (2009), and the ponding dye infiltration experiment performed in 2009. Kodešová et al. (2006b) discussed the impact of the variable shape factor (β = 3 and 15) and the characteristic length of the aggregates (a = 1 and 2.5 cm) on the one-dimensional numerical simulation of 1-h ponding infiltration into clay soils. They showed that a lower β value and a greater a value increased the final wetting front depth. In addition, a greater a value increased the irregularity of the wetting front shape (a

deeper progress of the wetting front in the macropore domain compared with that in the matrix domain). These parameters (at least in this case) influenced cumulative infiltration only marginally, however. Kodešová et al. (2009) used values of β = 5 and a = 0.2 cm to characterize small blocky aggregates. The ponding dye infiltration experiment performed in 2009 (Fig. 1) showed that water and the dye tracer moved mostly uniformly through the soil; however, some pore domains remained isolated. Therefore, several scenarios were simulated (see Table 2). The shape factor, β, was either 5 or 15 to allow study of the impact of the aggregate shape (blocky or spherical). The characteristic length of aggregates, a, was either 0.2 or 1.5 cm to simulate water flow in systems with either small (for a region with regular dye distribution and for a value assessed using the micromorphological images) or larger (for regions less impacted by dye tracer) aggregates.

The retention curve parameters (θ_r, θ_s, α and n) optimized for the laboratory ponding infiltration (PI inputs in Table 1) and K_s optimized for the tension disk infiltrometer experiment (Table 2, tension disk infiltrometer Replicate 1) were used to characterize the parameters ($\theta_{r,m}$, $\theta_{s,m}$, α_m, n_m, and $K_{s,m}$) of the matrix domain. The data from the laboratory ponding infiltration were chosen due to their similar experimental history (a wetting experiment). In addition, Gribb et al. (2004) showed that for sandy soils the shapes of hydraulic properties obtained using the cone permeameter (also an infiltration experiment and a flow domain geometry similar to that of the Guelph permeameter) were less gradual than those measured using an MSO experiment.

The parameters of the soil water retention curve for the macropore domain were set to ensure that macropores were filled with water only for pressure heads close to zero (a step-like shape curve). This assumption was clearly demonstrated in the analysis of bimodal soil water retention curves by Othmer et al. (1991). Previous studies also showed that the saturated water content of the macropore domain, $\theta_{s,f}$, may be the same as the $\theta_{s,m}$ of the matrix domain (Gerke and van Genuchten, 1996; Šimůnek et al., 2003; Kodešová et al., 2008, 2009) or larger (Gerke and Köhne, 2004; Gerke et al., 2007; Kodešová et al., 2006b, 2008), depending on the available data and parameter analysis. The residual soil water content of the macropore domain, $\theta_{r,f}$ was commonly assumed to be close to zero in these studies. The parameters α_f and n_f varied from 0.05 to 0.15 cm^{-1} and from 2 to 4, respectively. On the other hand, Vogel et al.

Table 2. Saturated hydraulic conductivities obtained from tension disk infiltrometer and Guelph permeameter tests.

Infiltration test	Soil-water retention curve parameters obtained from	Replicate 1		Replicate 2		Replicate 3		Avg. K_s	SD
		K_s	R^2	K_s	R^2	K_s	R^2		
		cm min^{-1}		cm min^{-1}		cm min^{-1}		cm min^{-1}	
Tension disk infiltrometer	ponding infiltration	1.25×10^{-4}	0.995	1.02×10^{-4}	0.999	0.92×10^{-4}	0.990	1.06×10^{-4}	0.57×10^{-9}
	multistep outflow	1.82×10^{-4}	0.998	1.53×10^{-4}	0.998	1.35×10^{-4}	0.994	1.57×10^{-4}	1.12×10^{-9}
Guelph permeameter	ponding infiltration	1.61×10^{-3}	0.999	1.07×10^{-3}	0.994	0.16×10^{-3}	0.980	9.47×10^{-4}	1.07×10^{-6}
	multistep outflow	1.66×10^{-3}	0.998	1.15×10^{-3}	0.990	0.21×10^{-3}	0.974	10.07×10^{-3}	1.08×10^{-6}

(2000), who did not assumed a step-like shaped soil water retention curve for the macropore domain, used the same soil water retention parameters in both domains. A one-dimensional numerical simulation of ponding infiltration (Kodešová et al., 2006b) indicated that $\theta_{s,f}$ influenced the wetting front depth but did not have a significant impact on cumulative infiltration. On the other hand, an increased α_f value (= 0.07 or 0.15) slightly decreased cumulative infiltration. As was expected, f_w and $K_{s,f}$ had the greatest impact on cumulative fluxes. Increasing values of these parameters resulted in increased cumulative infiltration and the wetting front moving to deeper depths. Because the fraction of the macropore domain was defined here as a ratio between the image porosity and the total porosity, $\theta_{s,f}$ was equal to $\theta_{s,m}$ (both equal to the measured porosity). This means that the total saturated soil water content was equal to the sum of the saturated soil water content of the matrix domain multiplied by its domain fraction (0.972), and the saturated water content of the macropore domain multiplied by its domain fraction (0.028). The residual water content of the macropore domain, $\theta_{r,f}$, was set to zero.

Since no independent measurements or predictions of α_f and n_f parameters were available, several scenarios were simulated to assess the impact of retention curve shape parameters (see Table 2). Parameter α_f was set to 0.05, 0.1, and 0.15 cm^{-1}. Parameter n_f was set to 2, 3, and 4. Simulations were performed only for $\beta = 15$ (spherical aggregates, which are usually expected in the Ap horizon) and $a = 0.2$ cm. Four scenarios (for all the scenarios described above) with various values of the effective saturated hydraulic conductivity, K_{sa} (Table 3), were studied. The first K_{sa} value was set to the value obtained by numerical inversion using the dual-permeability model in HYDRUS-1D (Kodešová et al., 2009). The other three values of K_{sa} were sequentially decreased by one order of magnitude.

The value of $K_{s,f}$ was calibrated manually because HYDRUS 2D/3D does not provide inverse capabilities for the dual-permeability

model. The objective function Φ, to be minimized during the parameter estimation process, was formulated using the cumulative infiltration, q (cm^3):

$$\Phi(\kappa, q) = \sum_{i=1}^{N} v_i \left[q^*(t_i) - q(t_i, \kappa) \right]^2 \qquad [6]$$

where κ is the vector of estimated parameters, N is the number of measurements of cumulative infiltration, $q^*(t_i)$ are specific measurements at time t_i, $q_i(t_i, \kappa)$ are the corresponding model predictions for parameter vector κ, and v_i is the weight associated with a particular measurement point ($v_i = 1$ for all data).

In addition, the possible impact of the less permeable plow pan (the Ap2 horizon) between depths of 25 and 35 cm was investigated. The same geometry structure parameters and soil hydraulic parameters as for the Ap1 horizon, except for the $K_{s,f}$ value, were assumed for this layer. The $K_{s,f}$ value was set lower (0.01 cm min^{-1}) compared with that in the Ap1 horizon. No impact on the estimated $K_{s,f}$ of the Ap1 horizon, simulated cumulative infiltration, or the shape of the wetting front was found. Therefore, these simulations are not discussed further.

Results and Discussion
Single-Porosity Model

The optimized K_s values, obtained using the single-porosity model by numerically inverting the data for three replications of both the tension disk infiltrometer and the Guelph permeameter experiments, are shown in Table 2. Different applied soil-water retention curve parameters (θ_r, θ_s, α, and n), which resulted from the previous MSO and PI tests (Table 1), noticeably affected the K_s values obtained from both experiments. In both cases, greater K_s values were obtained when the MSO parameters were used than when PI parameters were applied. The first reason for this is the lower MSO θ_s value and the subsequently larger initial relative saturation

Table 3. Saturated hydraulic conductivities of the macropore domain, $K_{s,f}$, correlation coefficients R^2, and objective functions Φ obtained for Test 1 with the Guelph permeameter for various scenarios with different effective saturated hydraulic conductivities of the interface between the two pore domains, K_{sa}, including aggregate shape factors, β, characteristic lengths of an aggregate, a, and the soil water retention parameters α and n of the macropore domain.

Scenario	β	a	α_f	n_f	$K_{sa} = 5.3 \times 10^{-5}$ cm min^{-1}			$K_{sa} = 5.3 \times 10^{-6}$ cm min^{-1}			$K_{sa} = 5.3 \times 10^{-7}$ cm min^{-1}			$K_{sa} = 5.3 \times 10^{-8}$ cm min^{-1}		
					$K_{s,f}$	R^2	Φ	$K_{s,f}$	R^2	Φ	$K_{s,f}$	R^2	Φ	$K_{s,f}$	R^2	Φ
		cm	cm^{-1}		cm min^{-1}			cm min^{-1}			cm min^{-1}			cm min^{-1}		
A	5	0.2	0.1	3	0.158	0.999	691.7	0.171	0.999	101.9	0.218	0.996	623.6	0.240	0.997	424.8
B	5	1.5	0.1	3	0.160	0.999	627.8	0.239	0.997	420.7	0.245	0.997	374.1	0.244	0.997	373.9
C	15	0.2	0.1	3	0.156	0.999	845.8	0.165	0.999	293.3	0.195	0.997	614.4	0.235	0.997	471.3
D	15	1.5	0.1	3	0.182	0.998	366.8	0.232	0.998	572.4	0.245	0.997	567.0	0.240	0.997	548.9
E	15	0.2	0.05	3	0.100	0.999	733.0	0.105	0.999	218.0	0.125	0.997	602.5	0.150	0.997	437.7
F	15	0.2	0.15	3	0.197	0.999	843.6	0.205	0.999	350.4	0.245	0.996	695.7	0.291	0.996	552.2
G	15	0.2	0.1	2	0.200	0.999	857.1	0.208	0.999	315.6	0.249	0.996	695.7	0.299	0.996	564.4
H	15	0.2	0.1	4	0.140	0.999	893.7	0.148	0.999	304.1	0.175	0.997	592.0	0.215	0.997	495.9

(given by the effective water content always calculated using the same initial soil water content and either MSO or PI values of θ_r and θ_s) for the MSO parameters than the PI parameters. The second reason is the more gradual shape of the retention curve when the MSO parameters were used, which resulted in faster flow and higher K_s values than when the PI parameters were used to simulate the same cumulative infiltration. Calculated differences between the K_s values obtained from the tension disk infiltrometer using either MSO or PI parameters (5.7×10^{-5} [Replicate 1], 5.1×10^{-5} [Replicate 2], and 4.3×10^{-5} cm min^{-1} [Replicate 3]) were similar to those calculated for the Guelph permeameter (5.0×10^{-5} [Replicate 1], 8.0×10^{-5} [Replicate 2], and 5.0×10^{-5} cm min^{-1} [Replicate 3]). While the K_s values obtained from the tension disk infiltrometer using MSO parameters were 1.45 (Replicate 1), 1.50 (Replicate 2), and 1.46 (Replicate 3) times higher than those using the PI parameters, however, the K_s values obtained from the Guelph permeameter using MSO parameters were only 1.03 (Replicate 1), 1.07 (Replicate 2), and 1.31 (Replicate 3) times higher than those using the PI parameters. The impact of different soil hydraulic properties on the predicted soil water content distributions for a single Guelph permeameter experiment (Replicate 1) is illustrated in Fig. 3. A more gradual shape of the soil water retention curve, with a lower value of the saturated soil water content obtained from the multistep outflow experiment (compared to the laboratory ponding infiltration), resulted in a deeper wetting front and more gradual soil water distributions.

The K_s values obtained from the Guelph permeameter were one order of magnitude higher than those obtained from the tension disk infiltrometer (Table 2). In addition, the analysis of three replicates for each scenario shows that the variability of the K_s values obtained using the Guelph permeameter is greater than that obtained using the tension disk infiltrometer. The greater K_s values obtained using the Guelph permeameter and their larger variability

may be explained by gravitational macropores. It has been shown in many studies (e.g., Jarvis, 2007), and it is demonstrated by the dye distribution in Fig. 1, that the presence of gravitational macropores considerably increases water and solute fluxes in soils under saturated conditions. Their occurrence depends on factors such as root system development, worm activity, and soil shrinking, and may thus vary significantly within the studied area. On the other hand, the K_s values obtained using the tension disk infiltrometer represent properties of the well-consolidated higher order aggregates (the matrix soil structure) at the end of the vegetative period, which reflect similar aggregation conditions and processes characteristic for a particular soil type and climate. As a result, experiments performed under unsaturated conditions could not aid in predicting K_s values characterizing saturated conditions in a soil with macropores.

The K_s values obtained from the tension disk infiltrometer (Table 2) were on the same order of magnitude as the K_s value obtained from the MSO experiment (Table 1). This similarity was probably caused by the fact that both experiments were performed primarily under unsaturated conditions, that is, when larger gravitational pores were not involved in water flow. The K_s values obtained from the Guelph permeameter experiments (Table 2) were closer to those obtained using laboratory ponding infiltration (Table 1). This was probably due to the fact that both experiments involved saturated conditions. The K_s values obtained from the Guelph permeameter, however, were one order of magnitude lower than those for the ponding infiltration. This difference may be caused by the spatial and temporal variability of gravitational pores in the Ap horizon or the possible closing or disruption of macropores during the drilling of the Guelph permeameter well (which could occur despite the precautions taken during the well preparation).

Dual-Permeability Model

The optimized K_s values obtained for all scenarios using the dual-permeability model by numerical inversion of data from the Guelph permeameter (Replicate 1) are shown in Table 3. Comparisons of Scenarios A with B and C with D show that larger calibrated $K_{s,f}$ values were obtained in all cases for the larger characteristic length of aggregates, $a = 1.5$ cm (Scenarios B and D), than for the lower $a = 0.2$ cm value (Scenarios A and C). In the case of the larger a value, a contact area between the matrix and macropore domains was smaller than for the lower a value. Therefore, for $a = 1.5$ cm, less water penetrated into the matrix domain from the macropore domain, and the wetting front in the macropore domain moved faster (higher $K_{s,f}$ values) and farther from the source compared with $a = 0.2$ cm, while at the same time
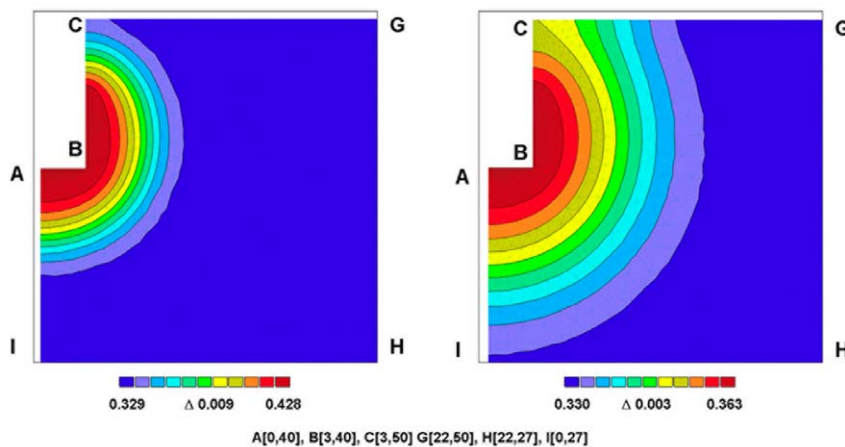

0.329   △ 0.009   0.428

0.330   △ 0.003   0.363

A[0,40], B[3,40], C[3,50] G[22,50], H[22,27], I[0,27]

Fig. 3. Final soil water contents (cm^3 cm^{-3}) for the Guelph permeameter test (Replicate 1), assuming the single-porosity model and soil water retention parameters obtained from the laboratory ponding infiltration (left) and the multistep outflow (right) experiments. Coordinates of the A, B, C, G, H, and I points in the radially symmetric system are in centimeters.

both scenarios produced the same cumulative infiltration as measured (Fig. 3). In addition, the lower mass exchange between both domains was compensated by the large direct cumulative infiltration into the matrix domain (from the infiltration well), as shown for $K_{sa} = 5.3 \times 10^{-6}$ cm min^{-1} (scenarios with the lowest values of the objective function) in Fig. 4.

Different saturations of the matrix and macropore domains at the end of the simulated infiltration (e.g., final wetting front positions) for the same K_{sa} value (= 5.3×10^{-6} cm min^{-1}) and Scenarios C and D are clearly documented in Fig. 5 and 6. The final soil water contents in the matrix and macropore domains are shown in Fig. 5 and 6, respectively. The final mass transfer between the macropore and matrix domains is presented in Fig. 7. It should be pointed out that the total soil water content is equal to the sum of the soil water contents of the matrix and macropore domains multiplied by their corresponding domain fractions (0.972 and 0.028). The figures show that pressure heads, and consequently the soil water contents, were more or less in equilibrium in both domains for scenarios with smaller aggregates and correspondingly faster mass exchange. Therefore, mass exchange occurred mainly at the wetting front of the macropore domain. On the other hand, for scenarios with larger aggregates, non-equilibrium in pressure heads between the two domains caused mass exchange throughout almost the entire flow domain impacted by macropore flow. Comparisons of Scenarios A with C and B with D show a very low impact of the aggregate shape parameter β (due to its small range of possible values) on the calibrated $K_{s,f}$ values. The $K_{s,f}$ values for β = 5 (except for scenarios with K_{sa} = 5.3 × 10^{-5} cm min^{-1}) were only slightly higher than those for β = 15. Figure 4 shows, however, that β evidently impacted more mass exchange between the macropore and matrix domains and the soil water content distribution for a = 1.5 cm than for a = 0.2 cm.

Comparisons of Scenarios E, C, and F demonstrate the impact of the α_f parameter (0.05, 0.1, and 0.15 cm^{-1}), which is frequently interpreted as an inverse value of the air-entry pressure head, on the calibrated $K_{s,f}$ values. Thus, a lower value of the α_f parameter produces an increased air-entry value and a correspondingly larger range of pressure heads for which the soil water contents and hydraulic conductivities are close to saturated values. Larger $K_{s,f}$ values were thus calibrated for the macropore domain characterized by a higher α_f to obtain the same measured cumulative infiltration. The limited impact of the α_f value on simulated cumulative fluxes for Scenarios C, E, and F with K_{sa} = 5.3 × 10^{-6} cm min^{-1} can be seen in Fig. 4. Wetting fronts for the same scenarios (for Scenario C shown in Fig. 5 [left] and 6 [left] and for Scenarios

E and F, which are not shown) moved in both regions to similar distances from the infiltration well. Water content distributions at the wetting front were slightly more gradual for a lower value of the α_f parameter.

Comparisons of Scenarios G, C, and H show the impact of the n_f parameter (= 2, 3, and 4) and the correspondingly increasing degree of the curve S-shape (from gradual to a step-like shape) on
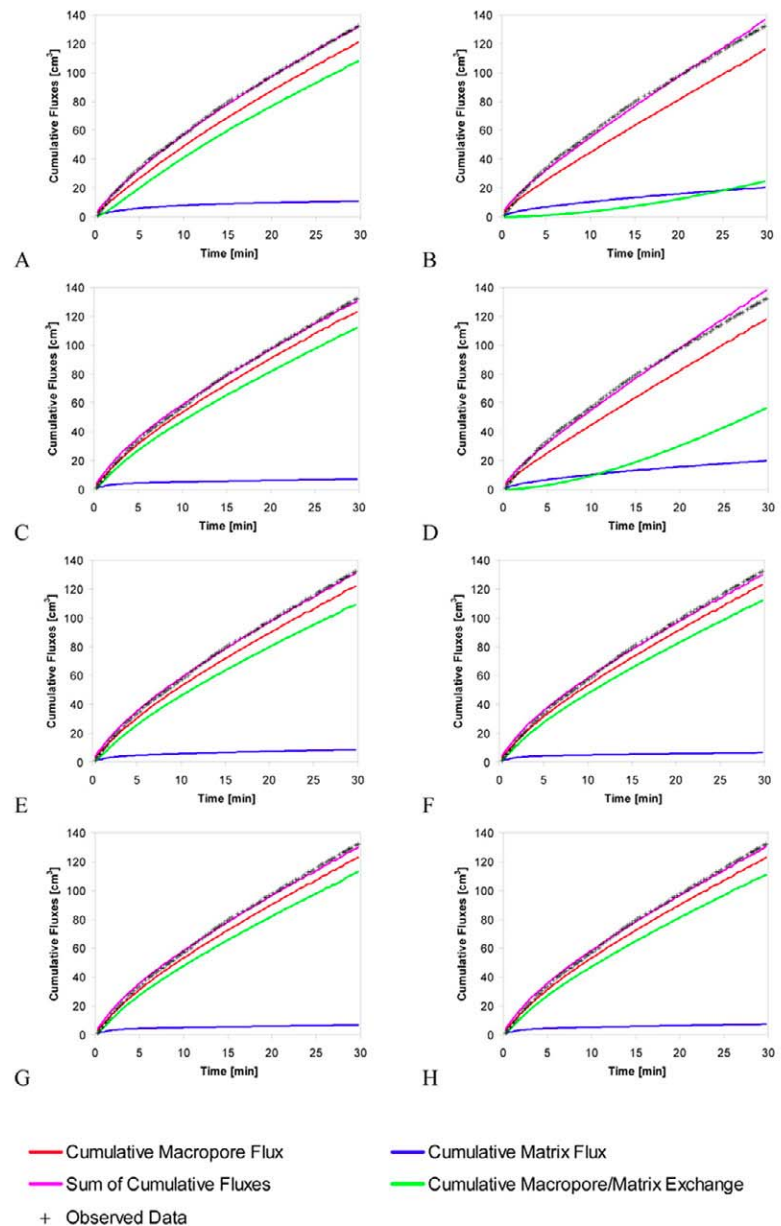

Fig. 4. Measured and simulated (using the dual-permeability model) cumulative infiltrations for the Guelph permeameter test (Replicate 1) for various scenarios (Table 3) and an effective saturated hydraulic conductivity of the interface between the two pore domains K_{sa} = 5.3 × 10^{-6} cm min^{-1}. Cumulative macropore flux is the direct (from the well) cumulative infiltration into the macropore domain; cumulative matrix flux is the direct cumulative infiltration into the matrix domain; sum of cumulative fluxes is the sum of the direct cumulative fluxes; cumulative macropore/matrix exchange is the cumulative infiltration from the macropore domain into the matrix domain.
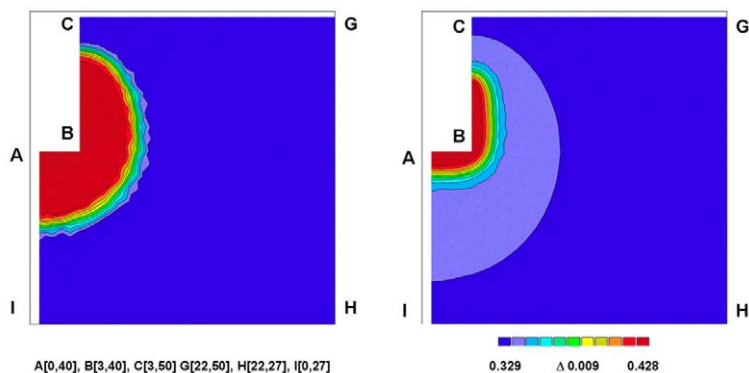
Fig. 5. Final soil water contents ($cm^3\ cm^{-3}$) in the matrix domain (simulated using the dual-permeability model) for the Guelph permeameter test (Replicate 1) for an effective saturated hydraulic conductivity of the interface between the two pore domains $K_{sa} = 5.3 \times 10^{-6}$ cm min^{-1} and for Scenarios B (left) and D (right). Coordinates of the A, B, C, G, H, and I points in the radially symmetric system are in centimeters.
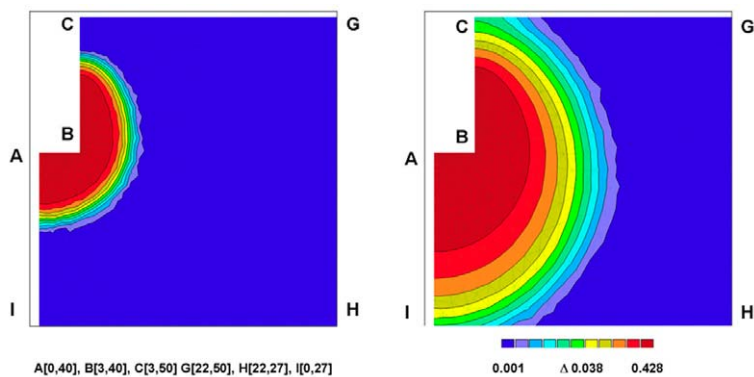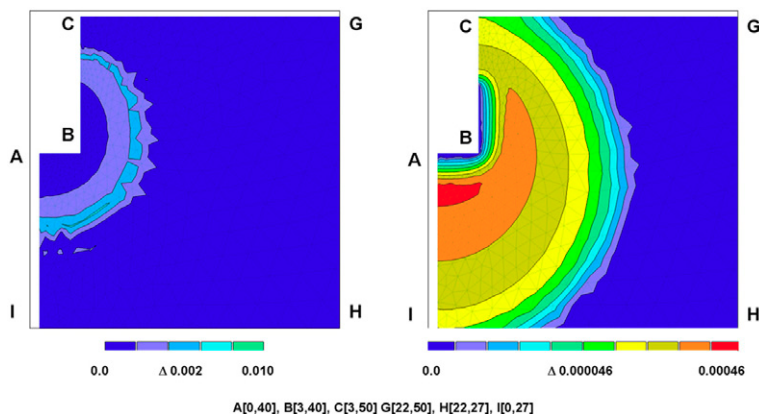

Fig. 6. Final soil water contents ($cm^3\ cm^{-3}$) in the macropore domain (simulated using the dual-permeability model) for the Guelph permeameter test (Replicate 1) for an effective saturated hydraulic conductivity of the interface between the two pore domains $K_{sa} = 5.3 \times 10^{-6}$ cm min^{-1} and Scenarios B (left) and D (right). Coordinates of the A, B, C, G, H, and I points in the radially symmetric system are in centimeters.

Fig. 7. Final mass transfer (min^{-1}) between the macropore and matrix domains (simulated using the dual-permeability model) for the Guelph permeameter test (Replicate 1) for an effective saturated hydraulic conductivity of the interface between the two pore domains $K_{sa} = 5.3 \times 10^{-6}$ cm min^{-1} and Scenarios B (left) and D (right). Coordinates of the A, B, C, G, H, and I points in the radially symmetric system are in centimeters.

calibrated $K_{s,f}$ values. As for increased air-entry pressure heads, the more step-like shape of the retention curve (i.e., higher n_f values) increased the range of pressure heads with soil water contents and hydraulic conductivities close to saturated values. Larger calibrated $K_{s,f}$ values were thus calibrated for the macropore domain characterized with lower n_f parameters. Again, Fig. 4 shows the limited impact of n_f on simulated cumulative fluxes for $K_{sa} = 5.3 \times 10^{-6}$ cm min^{-1}. Wetting fronts in both domains were again very similar in all cases (for Scenario C shown in Fig. 5 [left] and 6 [left] and Scenarios G and H, which are not shown). The lowest $K_{s,f}$ values were obtained for Scenario F and the largest $K_{s,f}$ values for Scenario G (for all K_{sa} values).

A comparison of results for different values of K_{sa} shows that $K_{s,f}$ increased with decreasing K_{sa} except for Scenarios B and D (for $a = 1.5$ cm). Almost the same $K_{s,f}$ values were obtained for K_{sa} values of 5.3×10^{-7} and 5.3×10^{-8} cm min^{-1}. Evidently, the reduction in the mass exchange between the macropore and matrix domains due to the aggregate size (discussed above) and low K_{sa} values was so high that cumulative infiltration was no longer influenced by the mass exchange. The impact of K_{sa} on particular cumulative infiltration fluxes is shown for Scenario A in Fig. 8. Figure 8 shows that relatively high exchange rates ($K_{sa} = 5.3 \times 10^{-5}$ and 5.3×10^{-6} cm min^{-1}) between the macropore and matrix domains reduced the simulated cumulative infiltration into the matrix domain and increased the cumulative infiltration into the macropore domain. On the other hand, lower exchange rates ($K_{sa} = 5.3 \times 10^{-7}$ and 5.3×10^{-8} cm min^{-1}) increased the cumulative infiltration into the matrix domain and decreased the cumulative infiltration into the macropore domain. As with the impact of aggregate size on mass transfer, the wetting front in the macropore domain moved faster (due to higher $K_{s,f}$ values) and farther from the source for lower values of K_{sa} than for higher values while producing the same cumulative infiltration as was measured.

The flow regimes for Scenario A and various K_{sa} values are documented in Fig. 9, 10, and 11. While the final soil water contents in the matrix and macropore domains are shown in Fig. 9 and 10, respectively, the final mass transfer between the macropore and matrix domains is presented in Fig. 11. Pressure heads, and consequently soil water contents, were more or less in equilibrium in both domains for K_{sa} values of 5.3×10^{-5} and 5.3×10^{-6} cm min^{-1} and correspondingly faster mass exchange (Fig. 9 and 10, top). Mass exchange for these scenarios took place close to the wetting front in the macropore domain. Figures 9 and 10 (bottom) for K_{sa} values of 5.3×10^{-7} and 5.3×10^{-8} cm min^{-1} show similar water content distributions in the matrix domain close to the Guelph permeameter well, which was largely

impacted by direct matrix infiltration. The faster flow and deeper percolation of the wetting front in the macropore domain, compared with the wetting front in the matrix domain, are clearly visible for scenarios with high K_{sa} values. While for the scenario with a K_{sa} value of 5.3×10^{-7} cm min^{-1}, the mass exchange between the macropore and matrix domains caused a small increase in water contents in the matrix domain at larger distances from the well, no visible (at least on the scale applied) increase in water contents was noticeable for the scenario with a K_{sa} value of 5.3×10^{-8} cm min^{-1}. Correspondingly, the final mass exchange was simulated for almost the entire flow region impacted by macropore flow in the former case, and almost no visible mass exchange was simulated for the latter case.

It is evident from the values of the calculated objective function that the best fit was obtained for Scenario A and K_{sa} = 5.3×10^{-6} cm min^{-1} (Φ = 101.9). Additionally, a considerably better fit was obtained using the dual-permeability model (Φ = 101.9) than the single-porosity model with the PI parameters (Φ = 835.0). It should be noted, however, that a better fit could be obtained for the single-porosity model using different θ_r, θ_s, α, and n parameters. For instance, the Φ value for the single-porosity model with the MSO parameters was only 192.4, but such gradual soil water retention curves are not characteristic for wetting experiments (Gribb et al., 2004). After comparing the water content distributions around the infiltration well simulated using the dual-permeability model (Fig. 9 and 10) with the results of the single-porosity model (Fig. 3), it is obvious that macropore flow and mass exchange between the two domains produced more uniform water content distributions.

Close correlation among parameters β, a, and K_{sa} reflects their direct effect on mass transfer (Eq. [3]). Independent evaluation of aggregate shape parameters is recommended because new imaging techniques, such as x-ray computed tomography, magnetic resonance, dye tracer, and micromorphological imaging (Köhne et al., 2009a; Kodešová, 2009), provide relatively reliable information about the soil structure. The K_{sa} value may also be independently evaluated. For instance, Gerke and Köhne (2002) measured the hydraulic properties of the aggregate skin from different adsorption rates between the aggregates with and without the skin. This method requires a spatial apparatus, however, and may be applied only for aggregates with well-developed skins. In addition, optimized K_{sa} values may compensate for the possible inaccuracies of independently determined a and β values.
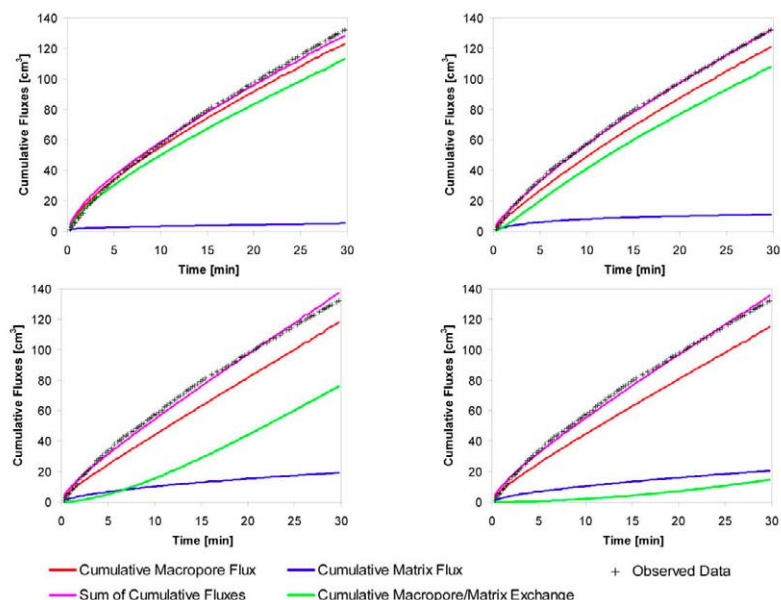

Fig. 8. Measured and simulated (using the dual-permeability model) cumulative infiltrations for the Guelph permeameter test (Replicate 1) for an effective saturated hydraulic conductivity of the interface between the two pore domains K_{sa} = 5.3×10^{-5} (top left), K_{sa} = 5.3×10^{-6} (top right), K_{sa} = 5.3×10^{-7} (bottom left), and K_{sa} = 5.3×10^{-8} cm min^{-1} (bottom right). Cumulative macropore flux is the direct (from the well) cumulative infiltration into the macropore domain; cumulative matrix flux is the direct cumulative infiltration into the matrix domain; sum of cumulative fluxes is the sum of the direct cumulative fluxes; cumulative macropore/matrix exchange is the cumulative infiltration from the macropore domain into the matrix domain.
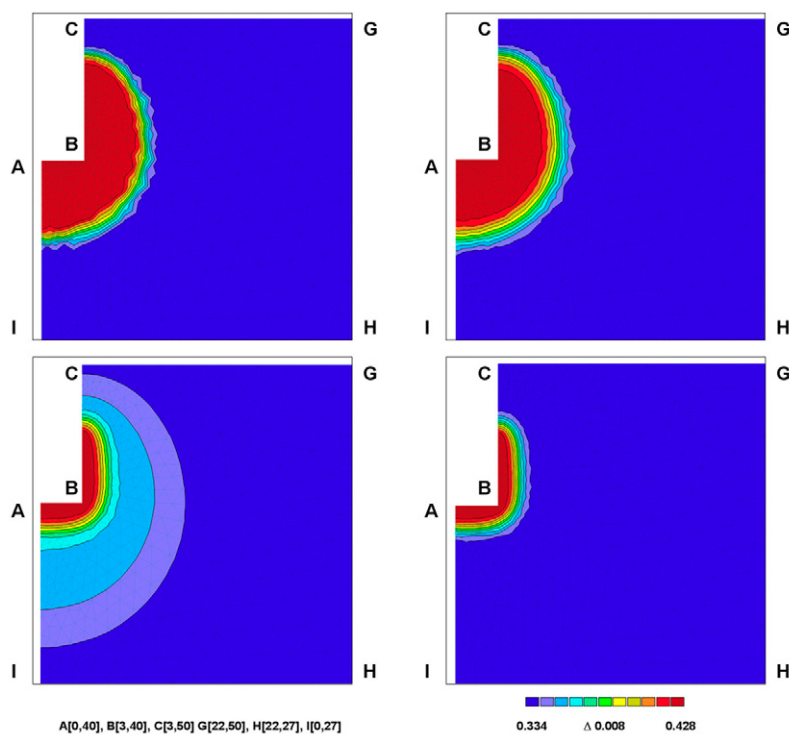

Fig. 9. Final soil water contents (cm^3 cm^{-3}) in the matrix domain (simulated using the dual-permeability model) for the Guelph permeameter test (Replicate 1) for an effective saturated hydraulic conductivity of the interface between the two pore domains K_{sa} = 5.3×10^{-5} (top left), K_{sa} = 5.3×10^{-6} (top right), K_{sa} = 5.3×10^{-7} (bottom left), and K_{sa} = 5.3×10^{-8} cm min^{-1} (bottom right), and for Scenario A. Coordinates of the A, B, C, G, H, and I points in the radially symmetric system are in centimeters.
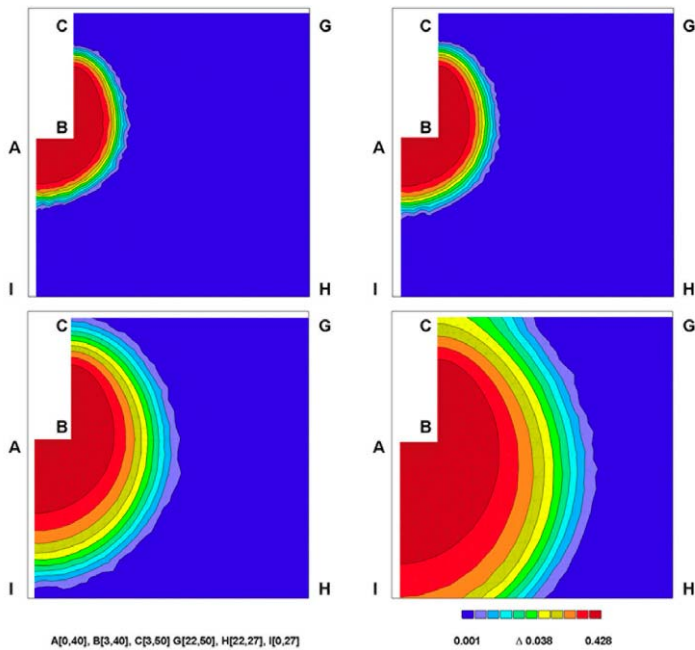
Fig. 10. Final soil water contents (cm^3 cm^{-3}) in the macropore domain (simulated using the dual-permeability model) for the Guelph permeameter test (Replicate 1) for an effective saturated hydraulic conductivity of the interface between the two pore domains $K_{sa} = 5.3 \times 10^{-5}$ (top left), $K_{sa} = 5.3 \times 10^{-6}$ (top right), $K_{sa} = 5.3 \times 10^{-7}$ (bottom left), and $K_{sa} = 5.3 \times 10^{-8}$ cm min^{-1} (bottom right), and for Scenario A. Coordinates of the A, B, C, G, H, and I points in the radially symmetric system are in centimeters.
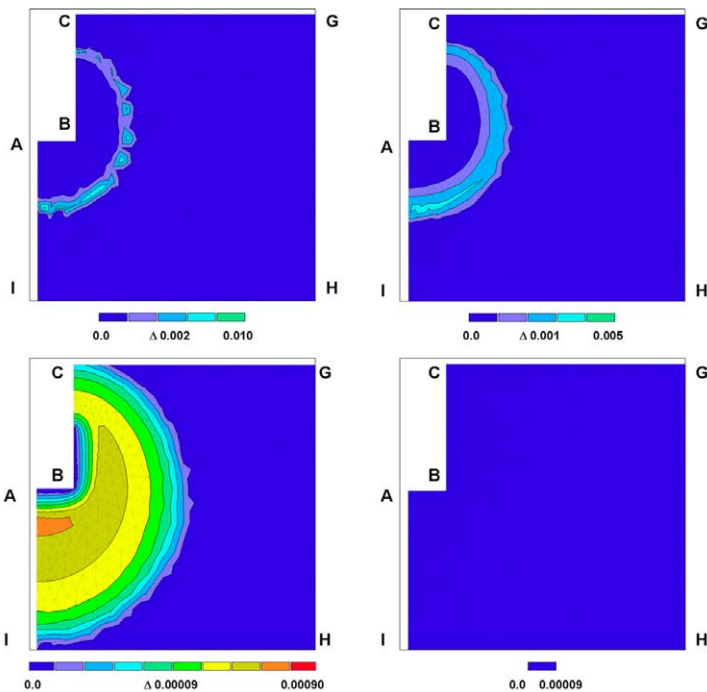

Fig. 11. Final mass transfer (min^{-1}) between the macropore and matrix domains (simulated using the dual-permeability model) for the Guelph permeameter test (Replicate 1) for an effective saturated hydraulic conductivity of the interface between the two pore domains $K_{sa} = 5.3 \times 10^{-5}$ (top left), $K_{sa} = 5.3 \times 10^{-6}$ (top right), $K_{sa} = 5.3 \times 10^{-7}$ (bottom left), and $K_{sa} = 5.3 \times 10^{-8}$ cm min^{-1} (bottom right) and for Scenario A. Coordinates of the A, B, C, G, H, and I points in the radially symmetric system are in centimeters.

♦ Conclusions

Tension disk infiltrometer and Guelph permeameter tests were used to estimate the saturated hydraulic conductivity, K_s, using the single-porosity model. It was shown that different soil water retention curves, obtained by either drying or wetting laboratory experiments, impacted the saturated hydraulic conductivities optimized from the field experiments. The K_s values obtained using parameters from the ponding infiltration experiment were suggested to better characterize the field experiments because this experiment represented a wetting process, and thus higher consistency was expected between them. In addition, greater K_s values were obtained from the Guelph permeameter tests than from the tension disk infiltrometer tests due to an occurrence of preferential flow caused by the gravitational pores. Therefore, the Guelph permeameter tests were used to estimate the saturated hydraulic conductivity of the macropore domain, K_{sf}, using the dual-permeability model.

The soil hydraulic parameters determined from the tension disk infiltrometer, obtained using the single-porosity model, were used as parameters for characterizing the matrix domain in the dual-permeability model. Since many parameters characterizing the dual-domain geometry, water retention in the macropore domain, and the effective saturated hydraulic conductivity of the domain interface were unknown and could not be estimated simultaneously, we have evaluated multiple scenarios with different fixed parameter sets. The use of these different parameter sets produced different estimates of K_{sf}. While the effective saturated hydraulic conductivities, K_{sa}, characterizing the exchange term hydraulic conductivity differed by orders of magnitude, however, the estimated saturated hydraulic conductivities of the macropore domain, K_{sf}, varied only within one order of magnitude (that is, within the natural range of spatial heterogeneity for the saturated hydraulic conductivity [Nielsen and Wendroth, 2003]). In addition, although simple infiltration experiments without additional measurements of transient flow data such as water contents or pressure heads in the soil are not expected to provide enough information for estimating other parameters (Šimůnek and van Genuchten, 1996), the objective function showed high sensitivity to at least two estimated parameters.

It is evident that the shape parameters of the soil water retention curve of the macropore domain influenced the estimated K_{sf} value. When no information is available about these parameters, however, the average α_f and n_f values may serve as reference values. It is possible that additional measurements of pressure heads in the soil may help improve parameter estimation. The impact of the aggregate shape parameter, β, was, in comparison with the effect of other parameters, very small. The characteristic length of aggregates, a, noticeably influenced the estimated K_{sf} values. Decreasing K_{sa} and increasing a similarly decreased mass transfer between the macropore and matrix

domains and subsequently caused a large nonequilibrium between the two domains and a large irregularity at the wetting front. Our results document the applicability of the approach presented for the assessment of some of these parameters (preferably K_{sf} and K_{sa}) of the dual-permeability model.

References

Ahuja, L.R., and C. Hebson. 1992. Root zone water quality model. GPSR Tech. Rep. 2. USDA-ARS Great Plains Syst. Res., Fort Collins, CO.

Chen, C., and R.J. Wagenet. 1992a. Simulation of water and chemicals in macropore soils: 1. Representation of the equivalent macropore influence and its effect on soil water flow. J. Hydrol. 130:105–126.

Chen, C., and R.J. Wagenet. 1992b. Simulation of water and chemicals in macropore soils: 2. Application of linear filter theory. J. Hydrol. 130:127–149.

Clothier, B.E., S.R. Green, and M. Deurer. 2008. Preferential flow and transport in soil: Progress and prognosis. Eur. J. Soil Sci. 59:2–13.

Freifeld, B.M., and C.M. Oldenburg. 2000. Restricted interval Guelph permeameter: Theory and application. Water Resour. Res. 36:1373–1380.

Gerke, H.H. 2006. Preferential flow descriptions for structured soils. J. Plant Nutr. Soil Sci. 169:382–400.

Gerke, H.H., J. Dušek, T. Vogel, and J.M. Köhne. 2007. Two-dimensional dual-permeability analyses of a bromide tracer experiment on a tile-drained field. Vadose Zone J. 6:651–667.

Gerke, H.H., and J.M. Köhne. 2002. Estimating hydraulic properties of soil aggregate skins from sorptivity and water retention. Soil Sci. Soc. Am. J. 66:26–36.

Gerke, H.H., and J.M. Köhne. 2004. Dual-permeability modeling of preferential bromide leaching from a tile-drained glacial till agricultural field. J. Hydrol. 289:239–257.

Gerke, H.H., and M.Th. van Genuchten. 1993. A dual-porosity model for simulating the preferential movement of water and solutes in structured porous media. Water Resour. Res. 29:305–319.

Gerke, H.H., and M.Th. van Genuchten. 1996. Macroscopic representation of structural geometry for simulating water and solute movement in dual-porosity media. Adv. Water Resour. 19:343–357.

Germann, P.F. 1985. Kinematic wave approach to infiltration and drainage into and from soil macropores. Trans. ASAE 28:745–749.

Germann, P. 1990. Preferential flow and generation of runoff: 1. Boundary layer flow theory. Water Resour. Res. 26:3055–3063.

Germann, P.F., and K. Beven. 1985. Kinematic wave approximation to infiltration into soils with sorbing macropores. Water Resour. Res. 21:990–996.

Gribb, M.M., R. Kodešová, and S.E. Ordway. 2004. Comparison of soil hydraulic property measurement methods. J. Geotech. Geoenviron. Eng. 130:1084–1095.

Hayashi, M., and W.L. Quinton. 2004. A constant-head well permeameter method for measuring field-saturated hydraulic conductivity above an impermeable layer. Can. J. Soil Sci. 3:255–264.

Jarvis, N.J. 1994. The MACRO model: Technical description and sample simulation. Rep. Diss. 19. Dep. of Soil Sci., Swedish Univ. of Agric. Sci., Uppsala.

Jarvis, N.J. 2007. Review of non-equilibrium water and solute transport in soil macropores: Principles, controlling factors and consequences for water quality. Eur. J. Soil Sci. 58:523–546.

Kodešová, R. 2009. Soil micromorphology use for modeling of a non-equilibrium water and solute movement. Plant Soil Environ. 55:424–428.

Kodešová, R., M.M. Gribb, and J. Šimůnek. 1998. Estimating soil hydraulic properties from transient cone permeameter data. Soil Sci. 163:436–453.

Kodešová, R., M. Kočárek, V. Kodeš, J. Šimůnek, and J. Kozák. 2008. Impact of soil micromorphological features on water flow and herbicide transport in soils. Vadose Zone J. 7:798–809.

Kodešová, R., V. Kodeš, A. Žigová, and J. Šimůnek. 2006a. Impact of plant roots and soil organisms on soil micromorphology and hydraulic properties. Biologia 61:S339–S343.

Kodešová, R., J. Kozák, and J. Šimůnek. 2006b. Numerical study of macropore impact on ponded infiltration in clay soils. Soil Water Res. 1:16–22.

Kodešová, R., S.E. Ordway, M.M. Gribb, and J. Šimůnek. 1999. Estimation of soil hydraulic properties with the cone permeameter: Field Studies. Soil Sci. 164:527–541.

Kodešová, R., N. Vignozzi, M. Rohošková, T. Hájková, M. Kočárek, M. Pagliai, J. Kozák, and J. Šimůnek. 2009. Impact of varying soil structure on transport processes in different diagnostic horizons of three soil types. J. Contam. Hydrol. 104:107–125.

Köhne, J.M., S. Köhne, and J. Šimůnek. 2006a. Multi-process herbicide transport in structured soil columns: Experiments and model analysis. J. Contam. Hydrol. 85:1–32.

Köhne, J.M., S. Köhne, and J. Šimůnek. 2009a. A review of model applications for structured soils: a) Water flow and tracer transport. J. Contam. Hydrol. 104:4–35.

Köhne, J.M., S. Köhne, and J. Šimůnek. 2009b. A review of model applications for structured soils: b) Pesticide transport. J. Contam. Hydrol. 104:36–60.

Köhne, J.M., B.P. Mohanty, and J. Šimůnek. 2006b. Inverse dual-permeability modeling of preferential water flow in a soil column and implications for field-scale solute transport. Vadose Zone J. 5:59–76.

Kool, J.B., and J.C. Parker. 1987. Development and evaluation of closed-form expressions for hysteretic soil hydraulic properties. Water Resour. Res. 23:105–114.

Mualem, Y. 1976. A new model for predicting the hydraulic conductivity of unsaturated porous media. Water Resour. Res. 12:513–522.

Nielsen, D.R., and O. Wendroth. 2003. Spatial and temporal statistics. Catena-Verlag, Reiskirchen, Germany.

Othmer, H., B. Diekkrüger, and M. Kutílek. 1991. Bimodal porosity and unsaturated hydraulic conductivity. Soil Sci. 152:139–149.

Philip, J.R. 1968. The theory of adsorption in aggregated media. Aust. J. Soil Res. 6:1–19.

Pot, V., J. Šimůnek, P. Benoit, Y. Coquet, A. Yra, and M.-J. Martinez Cordun. 2005. Impact of rainfall intensity on the transport of two herbicides in undisturbed grassed filter strip soil cores. J. Contam. Hydrol. 81:63–88.

Ramos, T.B., M.C. Gonçalves, J.C. Martins, M.Th. van Genuchten, and F.P. Pires. 2006. Estimation of soil hydraulic properties from numerical inversion of tension disk infiltrometer data. Vadose Zone J. 5:684–696.

Sander, T., and H.H. Gerke. 2007. Preferential flow patterns in paddy fields using a dye tracer. Vadose Zone J. 6:105–115.

Schwartz, R.C., and S.R. Evett. 2002. Estimating hydraulic properties of a fine-textured soil using a disc infiltrometer. Soil Sci. Soc. Am. J. 66:1409–1423.

Šimůnek, J., N.J. Jarvis, M.Th. van Genuchten, and A. Gärdenäs. 2003. Review and comparison of models for describing non-equilibrium and preferential flow and transport in the vadose zone. J. Hydrol. 272:14–35.

Šimůnek, J., R. Kodešová, M.M. Gribb, and M.Th. van Genuchten. 1999. Estimating hysteresis in the soil water retention function from cone permeameter test data. Water Resour. Res. 35:1329–1345.

Šimůnek, J., and M.Th. van Genuchten. 1996. Estimating unsaturated soil hydraulic properties from tension disc infiltrometer data by numerical inversion. Water Resour. Res. 32:2683–2696.

Šimůnek, J., and M.Th. van Genuchten. 1997. Estimating unsaturated soil hydraulic properties from multiple tension disc infiltrometer data. Soil Sci. 162:383–398.

Šimůnek, J., and M.Th. van Genuchten. 2008. Modeling nonequilibrium flow and transport with HYDRUS. Vadose Zone J. 7:782–797.

Šimůnek, J., M.Th. van Genuchten, and M. Šejna. 2008. Development and applications of the HYDRUS and STANMOD software packages and related codes. Vadose Zone J. 7:587–600.

Soilmoisture Equipment Corp. 2008. Model 2800K1 Guelph Permeameter Operating Instructions. Soilmoisture Equipment Corp., Santa Barbara, CA.

van Genuchten, M.Th. 1980. A closed-form equation for predicting the hydraulic conductivity of unsaturated soils. Soil Sci. Soc. Am. J. 44:892–898.

Vogel, T., H.H. Gerke, R. Zhang, and M.Th. van Genuchten. 2000. Modeling flow and transport in a two-dimensional dual-permeability system with spatially variable hydraulic properties. J. Hydrol. 238:78–89.

Watson, K.W., and R.J. Luxmoore. 1986. Estimating macroporosity in a forest watershed by use of a tension infiltrometer. Soil Sci. Soc. Am. J. 50:578–582.

Wooding, R.A. 1968. Steady infiltration from a shallow circular pond. Water Resour. Res. 4:1259–1273.

Zhang, Z.F., P.H. Groenevelt, and G.W. Parkin. 1998. The well-shape factor for the measurement of soil hydraulic properties using the Guelph permeameter. Soil Tillage Res. 49:219–221.

Zimmerman, R.W., T. Hadgu, and G.S. Bodvarsson. 1996. A new lumped-parameter model for flow in unsaturated dual-porosity media. Adv. Water Resour. 19:317–327.